Functionalization of Luminescent Aminated Particles for Facile Bioconjugation

Anne-Charlotte Faure,[†] Céline Hoffmann,[‡] Rana Bazzi,[†] Fabrice Goubard,[§] Emmanuel Pauthe,[‡] Christophe A. Marquette,[∥] Loïc J. Blum,[∥] Pascal Perriat,[#] Stéphane Roux,[†,*] and Olivier Tillement.[†]

[†]Laboratoire de Physico-Chimie des Matériaux Luminescents, UMR 5620 CNRS — Université Claude Bernard Lyon 1, 69622 Villeurbanne Cedex, France, [‡]Equipe de Recherche sur les Relations Matrice Extracellulaire-Cellules, E.A. 1391- Université de Cergy-Pontoise, 95302 Cergy-Pontoise Cedex, France, [§]Laboratoire de Physico-chimie des Polymères et des Interfaces, E.A. 2528- Université de Cergy-Pontoise, 95301 Cergy-Pontoise Cedex, France, [∥]Institut de Chimie et de Biochimie Moléculaires et Supramoléculaires, UMR 5246 CNRS - Université Claude Bernard Lyon 1, 69622 Villeurbanne Cedex, France, and [#]Matériaux, Ingénierie et Sciences, UMR 5510 CNRS - INSA de Lyon, 69621 Villeurbanne Cedex, France

ABSTRACT For labeling proteins (streptavidin and fibronectin) by luminescent aminated nanoparticles, an interesting strategy that requires neither activation nor chemical pre- or post-treatment was explored. Because biomolecules are easily rendered luminescent after reaction with organic dyes carrying isothiocyanate moiety, phenylene diisothiocyanate (DITC) was used for covalently binding proteins onto luminescent hybrid gadolinium oxide nanoparticles whose ability to combine imaging and therapy was recently demonstrated.

KEYWORDS: nanoparticles · polysiloxane shell · bioconjugation · streptavidin · fibronectin

The need for the detection of biomolecules traces and for the real time follow up of the living machinery from subcellular scale to whole organism (as small animals) led to the development of a large panel of luminescent markers for biological labeling.[1−3] Many works emphasized on the great potential of luminescent nanoparticles. Luminescent properties can be an intrinsic feature of the particles like in the case of quantum dots or can stem from the presence of organic fluorophores or of luminescent rare earth ions onto or inside the particles. As the chemical composition and the luminescence mechanisms are different, each kind of particles has a preferential application field. For instance, quantum dots and rare earth based nanoparticles are very well suited for multicolor and long-term imaging since they are characterized by large absorption bands, narrow emission bands and a high photostability.[4−12] However, their use for in vivo imaging is restricted both in the case of QD and rare earth based nanoparticles but for different reasons. The high toxicity of Cd^{2+} ions contained in QD is effectively a serious handicap for their use in living organisms.[13−15] This problem could be overcome by their encapsulation in silica shell[16,17] or by the replacement of cadmium by manganese[18,19] or by the use of InP nanoparticles.[20] Concerning lanthanide ions, as the excitation wavelength is in the UV region and the low absorption capacity imposes a high fluence, the energy necessary to induce light emission from nanoparticles containing luminescent rare earth ions is too high to be compatible with in vivo application.[21−23] A first solution is to develop lanthanide-based biolabels that emit in the visible region by either up-conversion or down-conversion. Recent works demonstrate this potentiality by developing an assembly with nearly monodispersed nanophosphors of lanthanides based nanoparticles encapsulated into silica shell and their biological conjugation to chitosan, FITC avidin, and streptavidin.[24−26] Another strategy consists in the sensitization of rare earth ions with antenna. The association of rare earth ions with antenna which absorbs light in the visible domain and transfers the energy to the luminescent centers induces a more intense light emission with a higher excitation wavelength.[27−31] On the contrary, the recent demonstration that the encapsulation of organic fluorophores in silica particles or vesicles led to higher photostability allows envisaging their application for in vivo imaging or for the detection of small amount of biomolecules.[32−35] Moreover, a large color palette can be obtained by mixing several organic fluorophores in a same particle.[36,37] Based on the works of the research groups of van Blaaderen, Tan, and Wiesner, many different and reliable routes

*Address correspondence to roux@pcml.univ-lyon1.fr.

Received for review July 16, 2008 and accepted October 24, 2008.

Published online November 6, 2008.
10.1021/nn8004476 CCC: $40.75

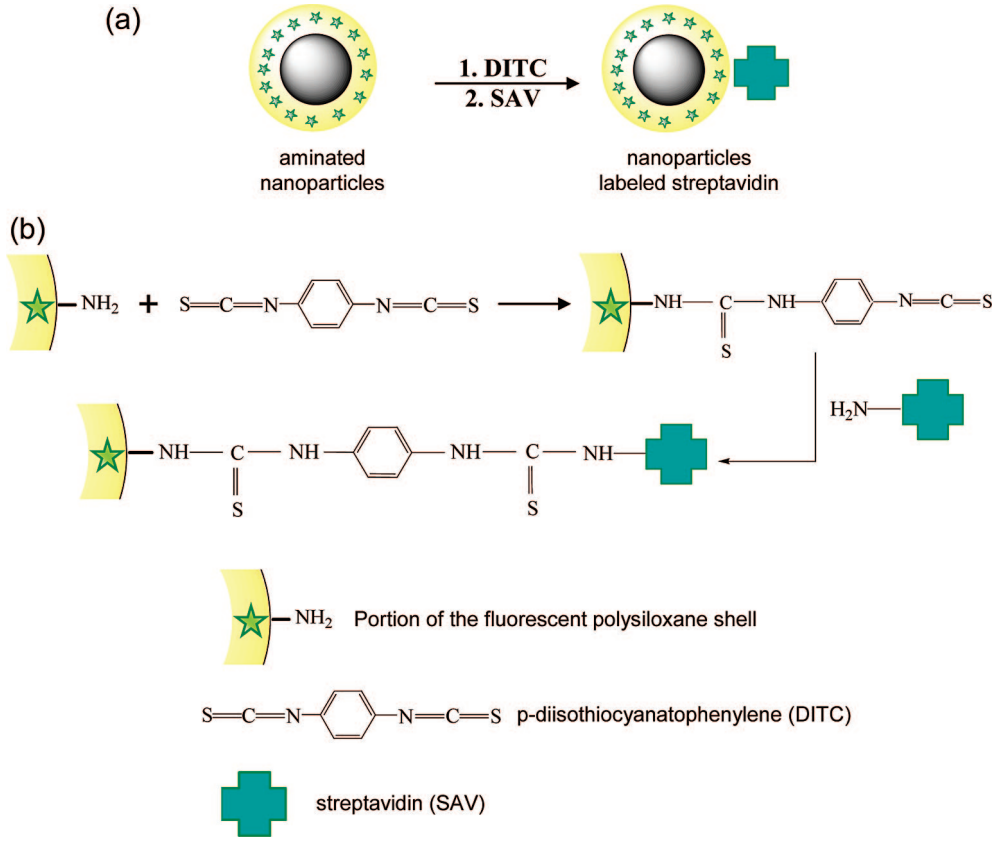

Scheme 1. (a) General principle of the grafting of streptavidin on aminated nanoparticles by using DITC; (b) detail of the covalent immobilization of streptavidin onto the aminated nanoparticles

for preparing luminescent silica particles have been described.[35,38,39] They were applied for encapsulating a large series of cores by luminescent polysiloxane shell. In most cases, the inorganic network is yielded by the hydrolysis−condensation of tetraethyl orthosilicate (TEOS) and aminopropyltriethoxysilane (APTES) or aminopropyltrimethoxysilane (APTMS). APTES and APTMS provide amino groups whose presence is crucial for the preparation of multifunctional nanoparticles. The functionalization of the nanoparticles or of the polysiloxane shell can be carried out sequentially since amino groups of APTES (or APTMS) can be coupled to various molecules *via* succinimidyl esters and isothiocyanates before and/or after the hydrolysis−condensation.[40−43] The modification of a part of APTES by fluorescent dyes carrying sulfonylchloride, NHS-ester, or isothiocyanate moieties before the hydrolysis condensation step allows a homogeneous repartition of the dyes within the particles, whereas the unmodified amino groups present on the surface can act as anchoring sites for the surface derivatization of the nanoparticles.[22,40−43] The immobilization of biomolecules on luminescent aminated nanoparticles can therefore be envisaged through an amide linkage. The formation of amide from an aminated surface requires the activation of the carboxylic acid moiety for improving the condensation yield. However, in the case of biomolecules containing several amino groups, in addition to the carboxylic acid functions, such activation can lead to their undesirable polymerization. Glutaraldehyde, which carries at both ends an aldehyde function, is also widely used for grafting aminated biomolecules onto aminated substrates.[44] However, a reduction step, which can be detrimental for the colloidal stability or for the integrity of the biomolecules, is required for converting the fragile imine linkages into resistant C−N bonds of secondary amines. Despite its very attractive feature, click chemistry can be penalized by the necessity of modifying the biomolecules by the acetylene derivative and the hazardous manipulation of azides.[45,46]

In this paper, an alternative way which consists in derivatizing the nanoparticles surface prior to the grafting of the biomolecules is reported. As isothiocyanate functions are able to easily react with amine without activation, the use of DITC which carries at both ends an isothiocyanate group appears very attractive for covalently linking the biomolecule to the aminated surface (Scheme 1). In this work, streptavidin and fibronectin were used to prove the possible bioconjugation of aminated luminescent nanoparticles derivatized by DITC. Streptavidin is pertinent owing to this specific and well-known high affinity recognition for biotin. Indeed, the avidin/biotin couple is well defined and usually used as a model for biomolecule detection.[47,48] Fibronectin is a large extracellular-matrix glycoprotein (550 kDa) found soluble in corporal fluids and immobi-

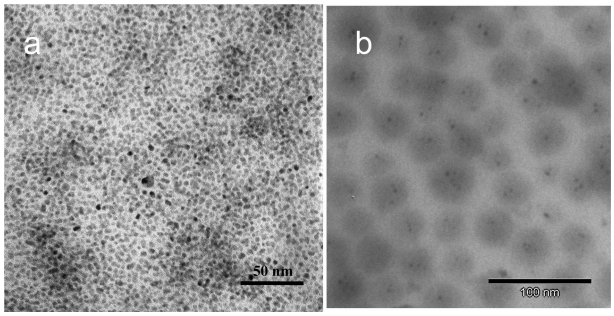

Figure 1. TEM images of Gd_2O_3 nanoparticles (a) before and (b) after polysiloxane shell growth.

lized in various tissues. The structure and stability of human plasmatic fibronectin are well-known and controlled.[49−51] This protein can specifically interact with many other proteins like collagen or heparin and is implicated in numerous physiological or pathological processes. Moreover, these proteins exhibit several amine moieties, which have been proved to react with isothiocyanate group because they can be rendered luminescent by the covalent immobilization of fluorescein isothiocyanate.[52] This work was carried out on nanoparticles composed of gadolinium oxide core embedded in a fluorescent polysiloxane shell because we recently demonstrated that these nanoparticles can be used as contrast agents for both fluorescence imaging and magnetic resonance imaging, but also as therapeutic agents.[43,53] Their great potential for biomedical applications will be plentifully exploited only if they can be selectively accumulated in zone of interest. This study appears, therefore, as a preliminary step for exploring efficient ways of the derivatization of nanoparticles by biotargeting groups.

RESULTS AND DISCUSSION

The labeling of streptavidin and fibronectin was performed with gadolinium oxide nanoparticles embedded in a fluorescent polysiloxane shell. These core−shell nanoparticles were obtained by applying a previously published two-step procedure.[22] First, well-dispersed 3 nm sized gadolinium oxide cores were synthesized by a polyol route (Figure 1a).

The growth of the fluorescent polysiloxane shell was controlled at 40 °C for 48 h by a sequential hydrolysis−condensation of a mixture of TEOS, APTES, and fluorescein or rhodamine conjugated APTES (40, 59.2, and 0.8%, respectively). TEM experiments show obviously the core−shell structure of the resulting nanoparticles (Figure 1b). It appears that each particle contains at least one core whose size is not altered by the shell growth.

This observation indicates that polymerization of the polysiloxane precursors occurred preferentially from the Gd_2O_3 core surface. Moreover, the preservation of the core size reflects the absence of agglomeration during the coating step. The resulting particles have a size around 35 nm (Figure 1b). Photon correlation spectroscopy (PCS) experiments which provide higher values for size than measurement from TEM images confirm that the size of the nanoparticles is 39 nm (mean standard deviation: 14 nm), whereas the size of the core is 3.8 nm (mean standard deviation: 0.4 nm; Figure 2). The increase of the size results from the encapsulation of the cores by a polysiloxane shell. The encapsulation induces a broadening of the size distribution which is inherent to the polymerization process (Figure 2). The incorporation of the fluorophores (FITC or RBITC) inside the polysiloxane shell is confirmed by the absorption and emission spectra of the colloids (Figure 3).

If the maximum absorption of free dyes and dyes covalently bound to the polysiloxane network of the fluorescent nanoparticles is almost located in the same spectral region (λ_{max} = 493 nm for FITC in the polysiloxane shell (Figure 3a) *versus* λ_{max} = 494 nm for free FITC and λ_{max} = 557 nm for RBITC in the polysiloxane shell (Figure 3b) *versus* λ_{max} = 554 nm for free RBITC), the maximum emission of dyes within polysiloxane shell is shifted toward higher wavelength (λ_{max} = 529 nm for FITC in the polysiloxane shell (Figure 3a) *versus* λ_{max} = 518 nm for free FITC and λ_{max} = 592 nm for RBITC in the polysiloxane shell (Figure 3b) *versus* λ_{max} = 575 nm for free RBITC). This arises from changes in

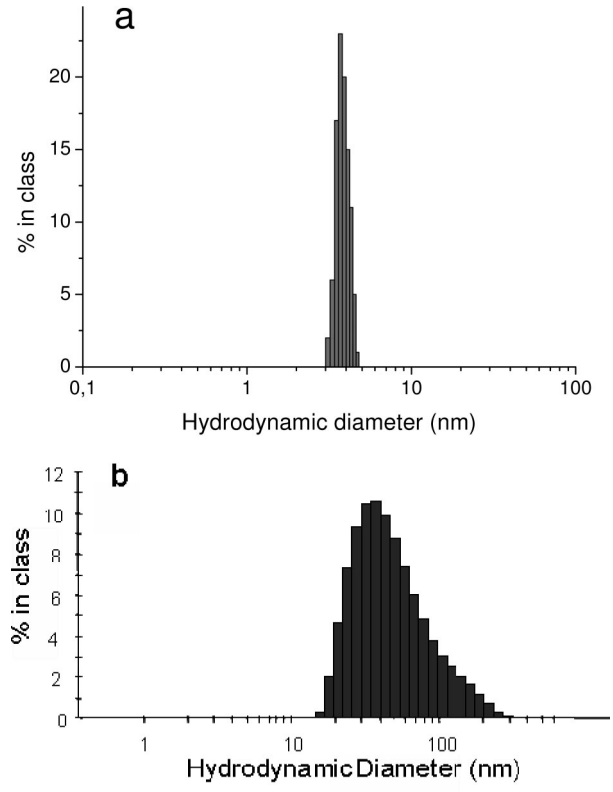

Figure 2. Size distribution determined by photon correlation spectroscopy of Gd_2O_3 nanoparticles (a) before and (b) after polysiloxane shell growth.

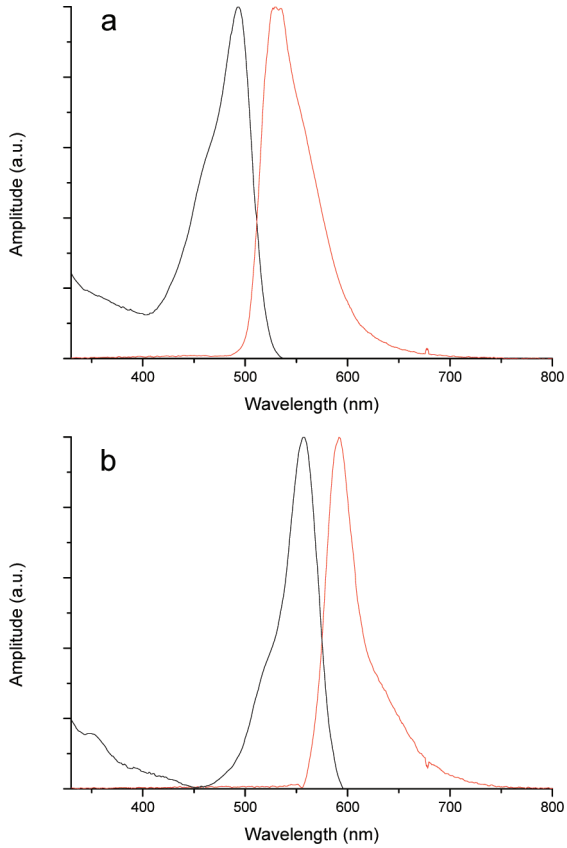

Figure 3. Absorption and emission spectra (black and red curves, respectively) of nanoparticles containing (a) FITC (λ_{exc} = 500 nm) and (b) RBITC (λ_{exc} = 554 nm) in water.

the environment of fluorophores and can be attributed to the incorporation of the organic dyes in the polysiloxane shell. Although mass spectrometry analyses demonstrated that all RBITC molecules are bound to APTES, the yield of incorporation is relatively low. The precipitation of nanoparticles induced by the addition of alkaline solution yields a colored supernatant. This results from the presence of the fluorophores, probably in the form of small fluorescent oligomers, which are not bound to the polysiloxane shell. After the removal of the colored supernatant, particles are easily redispersed in slightly acidic water. The resulting colloid is, as expected, less fluorescent. However, it must be pointed out that the fluorescence intensity of the colloid remains unchanged after further precipitation−redispersion cycles. This indicates that the coloration of the supernatant after the first addition of alkaline solution (which was never observed in the case of the following cycles) is attributed to ungrafted fluorescent entities. The alteration of the polysiloxane, which could induce the departure of fluorophores, can be consequently ruled out. Finally, the intensity of purified colloids is 4-fold weaker than crude colloids. In the case of FITC, cyanine 5, and porphyrins, the grafting yield is higher because fluorescence intensity is divided only by about two. Besides fluorescence imaging, we recently demonstrated that core−shell nanoparticles with gadolinium oxide core are well suited for *in vivo* MRI.[43] However, in this previous study, polysiloxane shell was thinner. Figure 4 displays the evolution of the longitudinal relaxation rate $1/T_1$ as a function of the gadolinium concentration. From the slope of the resulting straight line can be deduced the longitudinal relaxitivity r_1, which characterizes the ability of these particles to enhance the positive contrast of images acquired by MRI. Although the polysiloxane shell is relatively thick, these particles are able to enhance the positive contrast of MRI because they exhibit a longitudinal relaxivity r_1, which is equal to 3.8 $mM^{-1} \cdot s^{-1}$. This value is smaller than the one of the particles coated by a thin shell (3.8 *vs* 8.8 $mM^{-1} \cdot s^{-1}$). The decrease of r_1 can be assigned to the difficulty for water molecules to access to the surface of the core since the shell is thicker. However, it is similar to the one of DTPA-Gd, which is widely used for clinical diagnosis (3.8 *vs* 4.1 $mM^{-1} \cdot s^{-1}$).

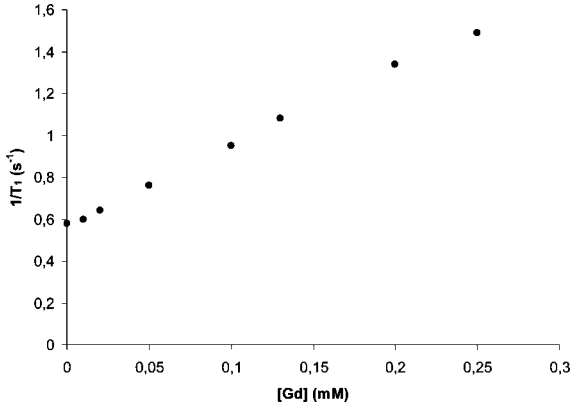

Figure 4. Water proton longitudinal relaxation rate ($1/T_1$) of the gadolinium oxide−polysiloxane core−shell nanoparticles as a function of increasing amounts of gadolinium element.

Because the polysiloxane shell is obtained from a mixture composed of a large portion of APTES, a large number of surface amino groups is expected. Their presence was revealed by ζ-potential measurements. Between pH 3 and 6, ζ-potential is almost constant and amounts to +6.4 mV. The positive charge of the particles that ensures the colloidal stability in slightly acidic water by electrostatic repulsion is attributed to the ammonium groups (NH_3^+), which are yielded by the protonation of NH_2 groups. For higher pH, precipitation is observed due to the deprotonation of ammonium groups. Higher colloidal stability in biological pH range (pH ∼ 7.4) is obtained by grafting carboxylated or aminated poly(ethylene glycol) chains (PEG). The latter ($PEG\text{-}NH_2$) is successfully immobilized by using DITC as cross-linker according to the protocol described in this manuscript for labeling streptavidin and fibronectin.

The reactive amino groups of core−shell particles are proven to be accessible for further functionalization. Indeed, we recently succeeded to immobilize on similar particles NHS-biotin and carboxylated poly(ethylene glycol) ($PEG\text{-}(COOH)_2$) *via* an amide linkage.[22,43]

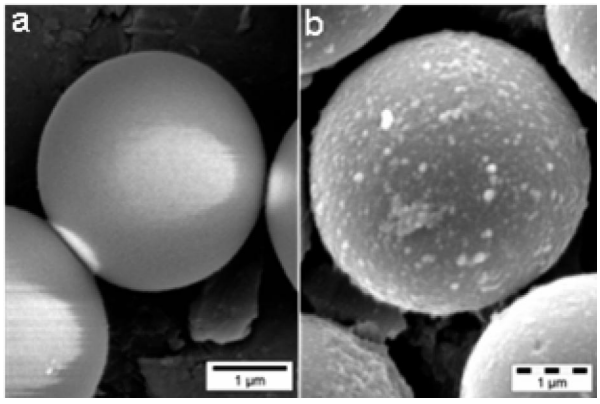

Figure 5. SEM images of biotinylated microspheres (a) before and (b) after incubation with nanoparticle-labeled streptavidin.

Biomolecules carrying carboxylic acid moiety should therefore be tethered to aminated surfaces. Nevertheless, the activation of the carboxylic acid moiety, which is required for improving the condensation yield, is not recommended when biomolecules contain several amino groups in addition to the carboxylic acid functions (case of proteins and peptides) because it can unfortunately lead to their undesirable polymerization. An alternative way consists in derivatizing the nanoparticles surface with DITC prior to the grafting of the biomolecules (streptavidin or fibronectin). DITC carries at both ends an isothiocyanate group and appears very attractive for covalently linking the biomolecule to the aminated surface because isothiocyanate functions are able to easily react with amine without activation (Scheme 1). When DITC is added to the amine-rich nanoparticles, one of the isothiocyanate moieties of DITC is expected to yield thiourea group after reaction with an amino group present on the particle, while the other one remains intact because the rigid structure of DITC should limit the bridging between two neighboring amino groups. As a result, the nanoparticles are covered by isothiocyanate groups, which will act as the anchoring site for biomolecules.

The immobilization of streptavidin or fibronectin needs, therefore, two steps: the conversion of the surface amino groups into surface isothiocyanate groups and the tethering of the biomolecule onto the nanoparticle. A total of 8 h after DITC addition to nanoparticles at room temperature, the latter were incubated with either streptavidin overnight or fibronectin for 1 h to obtain, through the formation of urea linkage, the labeling of streptavidin or fibronectin by the luminescent particles. Figure 5 shows that biotinylated silica microbeads exhibit higher roughness when they are incubated with nanoparticles after the reaction with DITC and streptavidin. This results from the immobilization of the nanoparticles on the microbeads. The presence of these nanoparticles confers to the beads a fluorescence that is characteristic of rhodamine (Figure 6). Both observations seem indicate the presence of streptavidin on the nanoparticles whose strong and specific interaction with biotin allows the immobilization of the luminescent nanoparticles on the beads.

Biochips and commercially available fluorescein-conjugated streptavidin were also used to confirm that streptavidin was successfully grafted to luminescent-aminated nanoparticles that contain within the polysiloxane shell rhodamine as dye. The chips are composed of an array of spots, each containing 1 μm latex beads partially inserted in a PDMS matrix.[54] The spotting pattern shows how the spots are distributed on each chip delineated by a white frame (Figure 7a). In the spots B, the beads are biotinylated for the recognition of streptavidin-coated luminescent hybrid particles by specific binding, whereas the latex beads of the spots X (called negative control) are unable to specifically fix the nanoprobes because they are devoid of biotin. For each biochip, two different signal acquisitions were performed to evidence either the FITC (fluorescein) luminescence (excitation, 280 nm; emission, 512 nm) or the RBITC (rhodamine) one (excitation, 490 nm; emission, 605 nm). Figure 7b and d correspond to the same biochip incubated in presence of luminescent nanoparticles after reaction with FITC labeled streptavidin, whereas Figure 7c and e display the same biochip incubated in presence of the fluorescein-conjugated streptavidin. Each biochip was visualized at $\lambda = 512$ nm (Figure 7b and c) and $\lambda = 605$ nm (Figure 7d and e) to evidence the presence of the two dyes. The efficiency of the biochip was demonstrated by using fluorescein-conjugated streptavidin (Figure 7c and e).

Due to the specific interaction between streptavidin and biotin, biotinylated spots B emitted, as expected, a green light (characteristic of fluorescein), whereas no light is detected from spots X (Figure 7c). Because the emission wavelength of fluorescein is around 515 nm, biotinylated spots are naturally not visible when only the light with $\lambda = 605$ nm (correspond-

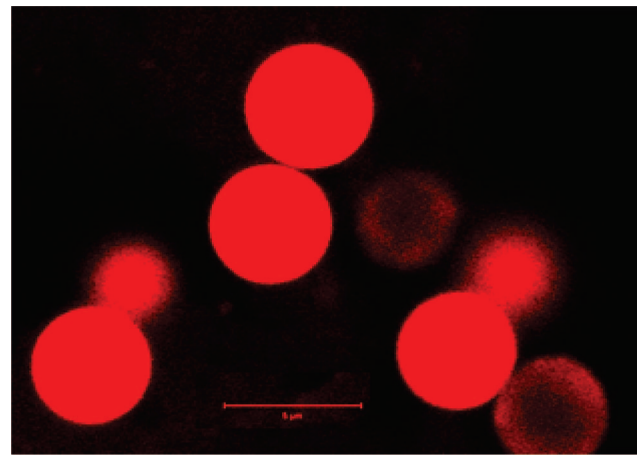

Figure 6. Confocal microscope image of biotinylated microspheres after incubation with nanoparticle-labeled streptavidin (scale bar = 5 μm).

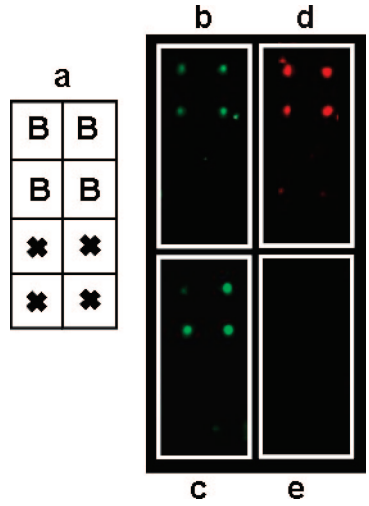

Figure 7. (a) Spotting pattern of the biochip (B for biotinylated spots and X for spot without biotin). Images of biochips incubated with nanoparticles after reaction with DITC and with FITC-conjugated streptavidin (b,d) and with FITC-conjugated streptavidin (c,e) under illumination (b,c) at 280 nm for recording FITC signal (λ_{em} = 512 nm) and (d,e) at 490 nm for recording RBITC signal (λ_{em} = 605 nm).

ing to RBITC emission) is collected after excitation at 490 nm (Figure 7e). The biochip incubated in the presence of hybrid particles encapsulating rhodamine in the polysiloxane shell and expected to be grafted to fluorescein-conjugated streptavidin after DITC surface derivatization exhibits a similar appearance when the light is recorded at λ =512 nm (Figure 7b and c) but appears obviously different for recording at λ = 605 nm (Figure 7d and e). Indeed, a red light characteristic of rhodamine is emitted from the biotinylated spots whereas no light is emitted from negative control spots X (Figure 7d). From this observation, we can deduce that hybrid nanoparticles are specifically bound to the biotinylated spots. Moreover, the detection of fluorescein (green light collected at λ = 512 nm) and of rhodamine (red light collected at λ = 605 nm) only on spots B reveals that the fluorescein-conjugated streptavidin and the rhodamine encapsulated within particles are localized in the same place. This colocalization is a second proof that streptavidin is effectively conjugated to hybrid nanoparticles. Precisely, this experiment demonstrates that (i) luminescent hybrid gadolinium oxide nanoparticles are successfully functionalized by streptavidin; (ii) the grafting of streptavidin on nanoparticles does not affect the behavior of streptavidin; and (iii) streptavidin-coated nanoparticles exhibit specific immobilization. For verifying the absence of the polymerization of the streptavidin during the labeling step, experiments on biochips were carried out with various concentrations of streptavidin labeled by fluorescent nanoparticles (Figure 8a). After incubation, biochips were immersed in a solution containing streptavidin conjugated peroxidase to detect free and accessible biotin on biochips (*i.e.*, biotin, which is not engaged in the interaction with streptavidin labeled by nanoparticles). The interaction of the streptavidin with free biotin led to the immobilization of the peroxidase. This enzyme is well-known for inducing the emission of light by catalyzing the oxidation of chemiluminescent luminol. Because the intensity of light emitted by luminol is proportional to the quantity of peroxidase on the biochip, the intensity reflects the amount of free biotin. The RBITC fluorescence intensity decreases with the dilution of the colloid (Figure 8a). As expected, the dilution induces the decrease of the amount of nanoparticles specifically immobilized onto the biochips through the interaction between biotin and streptavidin conjugated to the nanoparticles. Meanwhile, the amount of free and accessible biotin on biochips increases with the dilution of the colloid (Figure 8b) because the luminescence intensity increases gradually with the dilution. Assuming that the luminescence intensity of luminol measured after the incubation of a biochip only by streptavidin-conjugated peroxidase is proportional to the total amount of biotin contained in each spot of the

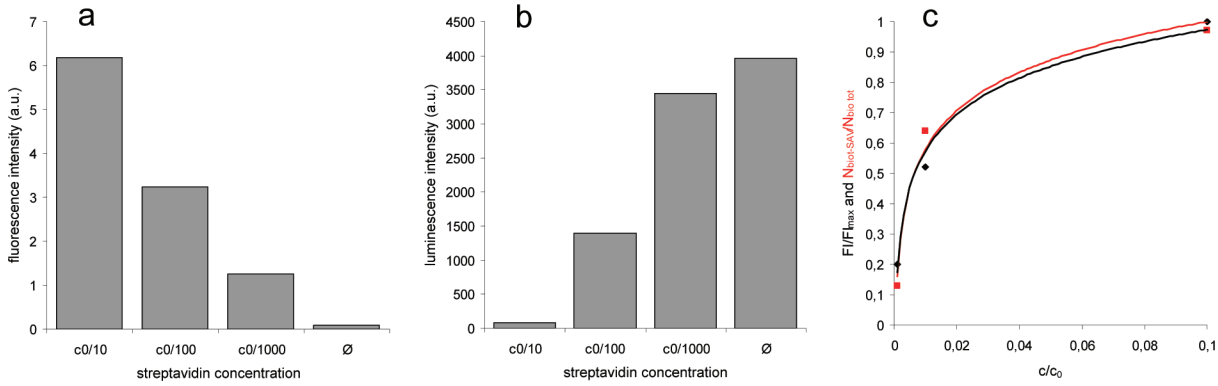

Figure 8. (a) Fluorescence intensity of a spot on a biochip after the incubation in colloid containing nanoparticles labeled streptavidin at various dilution rates. (b) Luminescence intensity of luminol after the incubation of the biochip with nanoparticles labeled streptavidin at various dilution rates and in a second step with streptavidin conjugated to peroxidase. (c) Normalized evolution of the fluorescence and of the amount of biotin bound to streptavidin labeled by a fluorescent nanoparticle (FI, fluorescence intensity; FI_{max}, fluorescence intensity for the lowest dilution rate; $N_{biot\text{-}SAV}$, amount of biotin bound to streptavidin labeled by a fluorescent nanoparticle; $N_{biot\ tot}$, total amount of free biotin before the incubation with the colloid of streptavidin labeled nanoparticles; *c*, concentration of streptavidin in the colloid; c_0, concentration of streptavidin in the stock colloid (*i.e.*, before the dilution)).

biochip, the measurement of luminescence intensity of a biochip, which was prior to the incubation with streptavidin-peroxidase immersed in the colloid, allows to determine the part of free biotin and consequently the part of biotin ensuring the specific immobilization of the nanoparticles through the interaction between streptavidin and biotin. Because the part of biotin bound to streptavidin labeled by nanoparticles and the normalized fluorescence intensity of the nanoparticles immobilized on the biochips exhibit a very similar evolution with the dilution (Figure 8c), we can assert that no polymerization of the streptavidin during the labeling step occurs.

The strategy based on the colocalization of different fluorescent markers was also exploited to validate the particles functionalization by fibronectin *via* DITC. Previous works demonstrated that fibronectin can be labeled by, at the most, 23 fluorescein isothiocyanate moieties due to the reaction of primary amine of the fibronectin and the isothiocyanate group of FITC.[52] Luminescent hybrid nanoparticles derivatized by DITC appear, therefore, very attractive for labeling fibronectin.

After the expected fixation of fibronectin to particles *via* DITC (see Methods), the fibronectin was extracted, deposited onto glass coverslip coated with gelatin and an immunofluorescent staining was performed. The examination of fibronectin with a fluorescent microscope reveals that the light emitted by fluorescein and by rhodamine can be selectively detected on the coverslip using appropriate filters under laser excitation (Figure 9a and b). Fluorescein, which is contained in the polysiloxane shell of the hybrid nanoparticles and rhodamine, which is conjugated to IgG, allows the localization of the particles and of fibronectin, respectively. Figure 9c results from the computational overlay of the micrographs of Figure 9a and b. An orange color is observed everywhere that fluorescein and rhodamine are colocalized. Because no more green and red spots but only orange spots can be distinguished, Figure 9c shows a perfect superimposition of the zones labeled by fluorescein and rhodamine. This indicates that all the fibronectin present on the coverslip and revealed by rhodamine owing to the immunostaining is grafted to nanoparticles containing fluorescein.

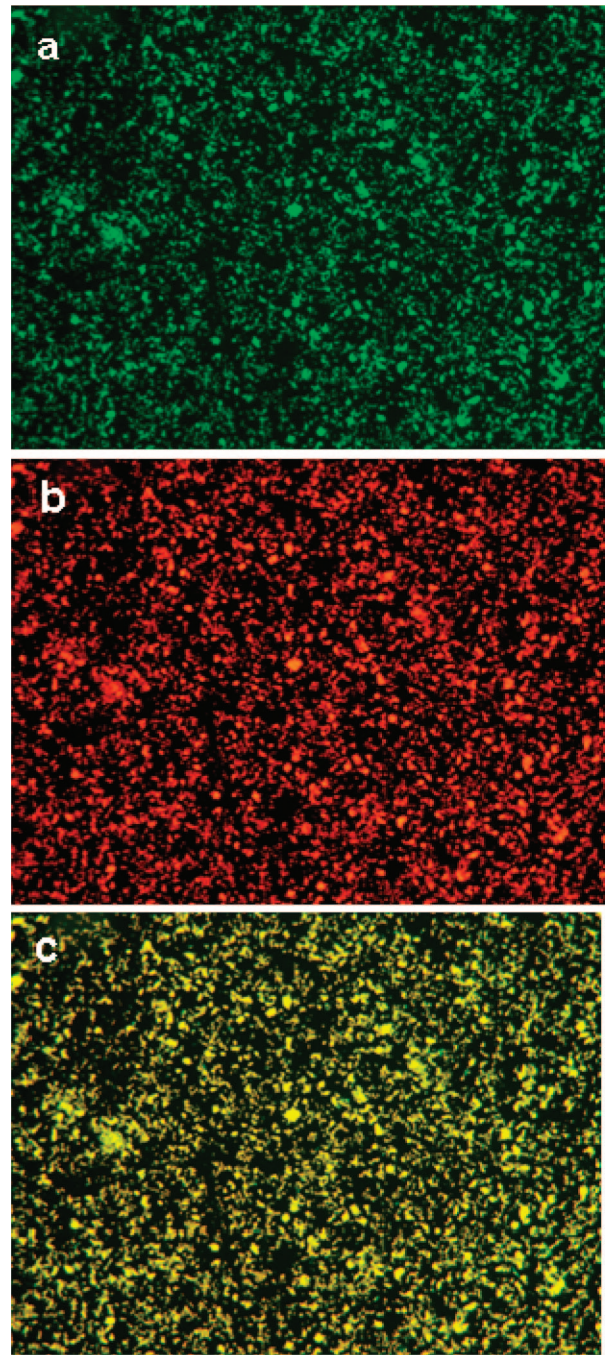

Figure 9. Fluorescence microscope images of nanoparticle-labeled fibronectin after incubation with antifibronectin antibody under laser excitation and with (a) FITC signal filter or (b) rhodamine B signal filter and (c) overlay of images (a) and (b).

CONCLUSION

The fluorescent detection of streptavidin and of the fibronectin was rendered possible thanks to their immobilization onto luminescent aminated nanoparticles composed of a gadolinium oxide core embedded in a polysiloxane shell. The labeling of these biomolecules was confirmed by colocalization experiments which consisted of labeling biomolecules with two different fluorescent probes (organic dyes or organic dyes conjugated antibodies (immunostaining) and luminescent hybrid nanoparticles). The functionalization of hybrid nanoparticles was revealed by the perfect superimposition of the zones containing each luminescent probe. These experiments demonstrated that DITC is, therefore, an efficient linker for tethering aminated nanoparticles to proteins. Because neither activation nor chemical pre- or post-treatment are required, this strategy appears very interesting for an alternative functionalization of nanoparticles coated by amine groups.

METHODS

Chemicals. Gadolinium chloride hexahydrate (99.99%), sodium hydroxide (99.99%), tetraethyl orthosilicate ($Si(OC_2H_5)_4$, TEOS, 98%), (3-aminopropyl)triethoxysilane ($H_2N(CH_2)_3$-$Si(OC_2H_5)_3$, APTES, 99%), fluorescein isothiocyanate (FITC, 90%), rhodamine B isothiocyanate (RBITC), hepes solution (solution in water, pH 7.0−7.6), triethylamine (TEA, 99.5%), dimethylsulfoxide, anhydrous dimethylsulfoxide (DMSO, 99.9%), *p*-phenylenediisothiocyanate (DITC), streptavidin, streptavidin-FITC, acetic acid, and dimethylformamide (DMF) were purchased from Aldrich Chemical (France). Phosphate buffer saline (PBS, 0.01 M phosphate buffer, 0.138 M NaCl, 0.0027 M KCl), Tween 20, and bovine serum albumin (BSA) were purchased from Sigma. Sodium chloride (NaCl) was purchased from VWR-Prolabo. Boric acid was purchased from Merck. Ethanol, diethylene glycol (DEG, 99%), and other organic solvents (reagent grade) were purchased from SDS (France) and used as received.

Encapsulation of Gd_2O_3 Cores in Polysiloxane Shell. A solution containing 3.2 mg of FITC or 4.4 mg of RBITC and 3.8 μL of APTES (m/z = 611.1, 721.2 for FITC- and RBITC-APTES, respectively) dissolved in 350 μL of ethanol or DMSO was prepared as a precursor and stirred overnight. This solution and a portion of 291.2 μL of APTES and of 187.4 μL of TEOS were added to 1 mL of solution containing Gd_2O_3 nanoparticles diluted in 9 mL of DEG under stirring at 40 °C. After 1 h, a portion of 714.3 μL of a DEG solution (0.1 M of triethylamine, 10 M of water) was added. The other portions of polysiloxane precursors and of hydrolysis solution were sequentially and alternatively added. The final mixture was stirred for 48 h at 40 °C.

Size Measurement. Direct measurement of the size distribution of the nanoparticles suspended in the polyol medium was performed via Zetasizer 3000 HSa and Zetasizer NanoS PCS (Photon Correlation Spectroscopy) from Malvern Instrument. Measurements were directly taken on the colloid after synthesis or surface modification.

ζ-Potential Measurements. Direct determination of the ζ-potential of the hybrid nanoparticles were performed via a Zetasizer NanoZS (laser He−Ne (633 nm)) from Malvern Instrument. Prior to the experiment, the sol was diluted in an aqueous solution containing 0.01 M NaCl and adjusted to the desired pH.

Absorption and Emission Spectra. Absorption and emission spectra were acquired on WPA spectrophotometer and on fluorescence spectrometer F2500 Hitachi, respectively.

Relaxation Time Measurements and MR Imaging. Relaxation time measurements were performed at 7 T using an inversion recovery FLASH (IR-FLASH) imaging sequence with varying IR time (Biospec System 70/20, Brucker, Ettlingen, Germany).

Fibronectin Preparation. Fibronectin (Fn) was purified from cryoprecipitated human plasma according to a protocol described by Poulloin *et al.* that yields a large quantity of homogeneous protein.[55] This protocol is based on the affinity of Fn for both gelatin and heparin. Briefly, the protocol consists in a combination of gelatin and heparin affinity chromatography steps. The purity of the preparation was estimated by densitometry analysis of silver nitrate-stained SDS-polyacrylamide gels (98.2 ± 0.8% (w/w). Fn concentrations were determined by optical absorbance measurements at 280 nm: $A_{1\%}$ = 12.8. Purified Fn is conserved in T10, pH 7.4 (10 mM Tris-HCl), at the concentration of 2 mg/mL at 10 °C.

Nanoparticles Bioconjugation. The *p*-phenylenediisothiocyanate is used as cross-linker between free primary amine groups from nanoparticles surface and amine containing biomolecule. Briefly, 18 μL of DITC dissolved in DMSO at a concentration of 10 mg/mL and 500 μL of Np in DEG solution (7.5 μM) are mixed. After 8 h of stirring at room temperature, 90 μL of streptavidin or FITC-conjugated streptavidin in 0.1 M borate buffer (pH 8.5; 2.5 mg/mL) or 2.07 mg of fibronectin, respectively, is added. This solution is allowed to react overnight at 4 °C in the case of streptavidin or only for 1 h at room temperature for fibronectin to prevent its denaturation by solvent. Coupled fibronectin is purified by centrifugation after dilution in a mixture of Tween 0.1%, BSA 1%, and NaCl 1 M. Fibronectin-pellet is conserved whereas the supernatant is replaced by the Tween mixture. Free nanoparticles in suspension are then progressively separated from fibronectin.

Fluorescence Imaging. Coverslips were homogenously coated by a gelatin solution at 50 μg/mL in PBS pH 7.4 for one night at RT and rinsed three times with PBS. Then, nanoparticle-labeled fibronectin is deposited onto gelatin coverslips over a period of 12 h at 4 °C. Immunofluorescent detection of Fn was performed as follows. Coated coverslips were saturated for 30 min in PBS-0.5% BSA and were then incubated for 1 h at room temperature in a dark humidified chamber with rabbit antihuman plasma fibronectin polyclonal antibody (Sigma, F-3648) diluted 1:50 in PBS-0.5% BSA. After three washings with PBS-0.5% BSA, coverslips were incubated for 1 h and 30 min with goat antirabbit IgG TRITC-conjugate antibody (Sigma, T-6678) diluted 1:50 in PBS-0.5% BSA. Coverslips were washed three times in PBS-0.5% BSA and one time in H_2O. Finally, the coverslips were mounted with Mowiol (Calbiochem) and examined with a fluorescent microscope (Leica MPS 60, 100W halogen lamp).

Biochip Preparation. The biochips were prepared by arraying 1.2 nL drops of spotting solutions with a BioChip Arrayer BCA1 (Perkin Elmer). The spotting solutions were prepared by mixing 100 μL of an aqueous solution composed of glycerol 2.5% and NaCl 0.05 M with 10 μL of an aqueous suspension of 1 μm biotinylated beads (1% w/v) purchased from Sigma (France). Each array was composed of eight spots (4 × 2) that were spotted at the surface of a 3D Teflon master composed of 24 rectangular structures (w = 5 mm, l = 5 mm, h = 1 mm). After spotting, the spots were dried and the arrays were transferred to a PDMS interface by pouring a mixture of precursor and curing agent (10:1) onto the Teflon substrate and cured for 5 min at 90 °C. The biochip preparation was then terminated by peeling off the PDMS polymer. The 3D structure resulting from this process produces a 24-well PDMS microarray (inner volume, 20 μL), exhibiting the 8-spot array at its bottom. All incubations or washing steps for a particular array were then performed by depositing a 20 μL solution volume into the wells.

Silica Microspheres Synthesis. Silica particles (4 μm) are obtained by a process described by De *et al.*[56] It consists in a microemulsion of tetraethoxysilane (TEOS) in acidic medium. Briefly, 11.4 mL of acetic acid are diluted in 3.6 mL of water. TEOS (0.05 mol) is added to this solution under stirring. The mixture is allowed to react only for exactly 1 min. Increasing the reaction time leads to an increased polydispersity. A total of 30 min after the stirring was stopped, the particles are separated by centrifugation. Particles were successively washed twice by water and twice by ethanol. The microspheres were then dried at room temperature and in vacuum. The surface of the microspheres was derivatized by amine groups after the reaction with APTES in dimethylformamide at 120 °C for 12 h.

Immobilization of the Nanoparticles on the Microspheres. A total of 50 mg of microparticles are suspended in 5 mL of water under vigorous stirring over a period of 10 min. After adding 1 mg of a NHS-biotin in DMSO solution (1 mg/mL) the mixture is allowed to react at room temperature for 3 h. The solution is then centrifuged. The supernatant is changed three times against water to eliminate nongrafted biotin molecules, whereas precipitated functionalized particles are resuspended in 5 mL of water. They are mixed with 500 μL of previously prepared streptavidin conjugated nanoparticles under slow stirring. After one night, the microparticles are separated by centrifugation and washed three times by solvent exchange against water. The microparticles are finally resuspended in acetone or ethanol for microscopy experiments (SEM and fluorescence microscopy).

Confocal Microscopy. An ethanol suspension of purified functionalized microparticles was deposited onto a coverslip for their observation using a confocal microscope (Zeiss LSM510 META). Confocal microscopy was performed at the Centre Technologique des Microstructures of the University Claude Bernard Lyon 1.

Acknowledgment. This work was supported by the Agence Nationale de la Recherche (ANR-05-NANO-037−02).

REFERENCES AND NOTES

1. Cai, W.; Chen, X. Nanoplatforms for Targeted Molecular Imaging in Living Subjects. *Small* **2007**, *11*, 1840–1854.
2. Wang, L.; Wang, K.; Santra, S.; Zhao, X.; Hilliard, L. R.; Smith, J. E.; Wu, Y.; Tan, W. Watching Silica Nanoparticles Glow in the Biological World. *Anal. Chem.* **2006**, *78* (3), 646–654.
3. Seydack, M. Nanoparticle Labels in Immunosensing using Optical Detection Methods. *Biosens. Bioelectron.* **2005**, *20*, 2454–2469.
4. Agrawal, A.; Deo, R.; Wang, G. D.; Wang, M. D.; Nie, S. Nanometer-Scale Mapping and Single-Molecule Detection with Color-Coded Nanoparticles Probes. *Proc. Natl. Acad. Sci. U.S.A.* **2008**, *105* (9), 3298–3303.
5. Tada, H.; Higuchi, H.; Wanatabe, T. M.; Ohuchi, N. In Vivo Real-Time Tracking of Single Quantum Dots Conjugated with Monoclonal Anti-HER2 Antibody in Tumors of Mice. *Cancer Res.* **2007**, *67*, 1138–1144. *3*.
6. Medintz, I. L.; Uyeda, H. T.; Goldman, E. R.; Mattoussi, H. Quantum Dot Bioconjugates for Imaging, Labelling and Sensing. *Nat. Mater.* **2005**, *4*, 435–446.
7. Bruchez, M.; Moronne, M.; Gin, P.; Weiss, S.; Alivisatos, A. P. Semiconductor Nanocrystals as Fluorescent Biological Labels. *Science* **1998**, *281*, 2013–2016.
8. Bazzi, R.; Brenier, A.; Perriat, P.; Tillement, O. Optical Properties of Neodynium Oxides at the Nanometer Scale. *J. Lumin.* **2005**, *113*, 161–167.
9. Giaume, D.; Buissette, V.; Lahlil, K.; Gacoin, T.; Boilot, J.-P.; Casanova, D.; Beaurepaire, E.; Sauviat, M.-P.; Alexandrou, A. Emission Properties and Applications of Nanostructured Luminescent Oxide Nanoparticles. *Prog. Solid State Chem.* **2005**, *33*, 99–106.
10. Bazzi, R.; Flores-Gonzalez, M. A.; Louis, C.; Lebbou, K.; Zhang, W.; Dujardin, C.; Roux, S.; Mercier, B.; Ledoux, G.; Bernstein, E.; et al. Synthesis and Properties of Europium-Based Phosphors on the Nanometer Scale Eu_2O_3, Gd_2O_3:Eu, and Y_2O_3:Eu. *J. Colloid Interface Sci.* **2004**, *273*, 191–197.
11. Bazzi, R.; Flores-Gonzalez, M. A.; Louis, C.; Lebbou, K.; Dujardin, C.; Brenier, A.; Zhang, W.; Tillement, O.; Bernstein, E.; Perriat, P. Synthesis and Luminescent Properties of sub-5-nm Lanthanide Oxides Nanoparticles. *J. Lumin.* **2003**, *102−103*, 445–450.
12. Stouwdam, J. W.; Hebbink, G. A.; Huskens, J.; van Veggel, F. C. J. M. Lanthanide-Doped Nanoparticles with Excellent Luminescent Properties in Organic Media. *Chem. Mater.* **2003**, *15*, 4604–4616.
13. Kirchner, C.; Liedl, T.; Kudera, S.; Pellegrino, T.; Muñoz Javier, A.; Gaub, H. E.; Stölzle, S.; Fertig, N.; Parak, W. J. Cytotoxicity of Colloidal CdSe and CdSe/ZnS Nanoparticles. *Nano Lett.* **2005**, *5*, 331–338.
14. Hoshino, A.; Fujioka, K.; Oku, T.; Suga, M.; Sasaki, Y. F.; Ohta, T.; Yasuhara, M.; Suzuki, K.; Yamamoto, K. Physicochemical Properties and Cellular Toxicity of Nanocrystal Quantum Dots Depend on their Surface Modification. *Nano Lett.* **2004**, *4*, 2163–2169.
15. Derfus, A. M.; Chan, W. C. W.; Bhatia, S. N. Probing the Cytotoxicity of Semiconductor Quantum Dots. *Nano Lett.* **2004**, *4*, 11–18.
16. Bakalova, R.; Zhelev, Z.; Aoki, I.; Ohba, H.; Imai, Y.; Kanno, I. Silica-Shelled Single Quantum Dot Micelles as Imaging Probes with Dual or Multimodality. *Anal. Chem.* **2006**, *78*, 5925–5932.
17. Nann, T.; Mulvaney, P. Single Quantum Dots in Spherical Silica Particles. *Angew. Chem., Int. Ed.* **2004**, *43*, 5393–5396.
18. Pradhan, N.; Battaglia, D. M.; Liu, Y.; Peng, X. Efficient, Stable, Small, and Water-Soluble Doped ZnSe Nanocrystal Emitters as Non-Cadmium Biomedical Labels. *Nano Lett.* **2007**, *7*, 312–317.
19. Santra, S.; Yang, H.; Holloway, P. H.; Stanley, J. T.; Mericle, R. A. Synthesis of Water-Dispersible Fluorescent, Radio-Opaque, and Paramagnetic CdS:Mn/ZnS Quantum Dots: A Multifunctional Probe For Bioimaging. *J. Am. Chem. Soc.* **2005**, *127*, 1656–1657.
20. Bharali, D. J.; Lucey, D. W.; Jayakumar, H.; Pudavar, H. E.; Prasad, P. N. Folate-Receptor-Mediated Delivery of InP Quantum Dots for Bioimaging Using Confocal and Two-Photon Microscopy. *J. Am. Chem. Soc.* **2005**, *127*, 11364–11371.
21. Diamente, P. R.; Burke, R. D.; Van Veggel, F. C. J. M. Bioconjugation of Ln^{3+}-Doped LaF_3 Nanoparticles to Avidin. *Langmuir* **2006**, *22*, 1782–1788.
22. Louis, C.; Bazzi, R.; Marquette, C. A.; Bridot, J.-L.; Roux, S.; Ledoux, G.; Mercier, B.; Blum, L.; Perriat, P.; Tillement, O. Nanosized Hybrid Particles with Double Luminescence for Biological Labeling. *Chem. Mater.* **2005**, *17*, 1673–1682.
23. Tan, M.; Wang, G.; Hai, X.; Ye, Z.; Yuan, J. Development of Functionalized Fluorescent Europium Nanoparticles for Biolabeling and Time-Resolved Fluorometric Applications. *J. Mater. Chem.* **2004**, *14*, 2896–2901.
24. Chen, Z.; Chen, H.; Hu, H.; Yu, M.; Li, F.; Zhang, Q.; Zhou, Z.; Yi, T.; Huang, C. Versatile Synthesis Strategy For Carboxylic Acid-Functionalized Upconverting Nanophosphors as Biological Labels. *J. Am. Chem. Soc.* **2008**, *130*, 3023–3029.
25. Sivakumar, S.; Diamente, P. R.; van Veggel, F. C. J. M. Silica-Coated Ln^{3+}-Doped LaF_3 Nanoparticles as Robust Down- and Upconverting Biolabels. *Chem.—Eur. J.* **2006**, *12*, 5878–5884.
26. Wang, F.; Zhang, Y.; Fan, X. P.; Wang, M. Q. One-Pot Synthesis of Chitosan/LaF_3:Eu^{3+} Nanocrystals for Bioapplications. *Nanotechnology* **2006**, *17*, 1527–1532.
27. Charbonnière, L. J.; Rehspringer, J.-L.; Ziessel, R.; Zimmermann, Y. Highly Luminescent Water-Soluble Lanthanide Nanoparticles through Surface Coating Sensitization. *New J. Chem.* **2008**, *32*, 1055–1059.
28. Zhang, J.; Shade, C. M.; Chengelis, D. A.; Petoud, S. A Strategy to Protect and Sensitize Near-Infrared Luminescent Nd^{3+} and Yb^{3+}: Organic Tropolonate Ligands for the Sensitization of Ln^{3+}-Doped $NaYF_4$ Nanocrystals. *J. Am. Chem. Soc.* **2007**, *129*, 14834–14835.
29. Chen, Y.; Chi, Y.; Wen, H.; Lu, Z. Sensitized Luminescent Terbium Nanoparticles: Preparation and Time-Resolved Fluorescence Assay for DNA. *Anal. Chem.* **2007**, *79*, 960–965.
30. Louis, C.; Roux, S.; Ledoux, G.; Dujardin, C.; Tillement, O.; Cheng, B.; Perriat, P. Luminescence Enhancement by Energy Transfer in Core-Shell Structures. *Chem. Phys. Lett.* **2006**, *429*, 157–160.
31. Louis, C.; Roux, S.; Ledoux, G.; Lemelle, L.; Gillet, P.; Tillement, O.; Perriat, P. Gold Nano-Antennas for Increasing Luminescence. *Adv. Mater.* **2004**, *16*, 2163–2166.
32. Lin, Y.-C.; Tsai, C.-P.; Huang, H.-Y.; Kuo, C.-T.; Hung, Y.; Huang, D.-M.; Chen, Y.-C.; Mou, C.-Y. Well-Ordered Mesoporous Silica Nanoparticles as Cell Markers. *Chem. Mater.* **2005**, *17*, 4570–4573.
33. Lian, W.; Litherland, S. A.; Badrane, H.; Tan, W.; Wu, D.; Baker, H. V.; Gulig, P. A.; Lim, D. V.; Jin, S. Ultrasensitive Detection of Biomolecule with Fluorescent Dye-doped Nanoparticles. *Anal. Biochem.* **2004**, *334*, 135–144.
34. Zhao, X.; Tapec-Dytioco, R.; Tan, W. Ultrasensitive DNA Detection Using Highly Fluorescent Bioconjugated Nanoparticles. *J. Am. Chem. Soc.* **2003**, *125*, 11474–11475.
35. Santra, S.; Zhang, P.; Wang, K.; Tapec, R.; Tan, W. Conjugation of Biomolecules with Luminophore-Doped Silica Nanoparticles for Photostable Biomarkers. *Anal. Chem.* **2001**, *73*, 4988–4993.
36. Wang, L.; Tan, W. Multicolor FRET Silica Nanoparticles by Single Wavelength Excitation. *Nano Lett.* **2006**, *6*, 84–88.
37. Wang, L.; Yang, C.; Tan, W. Dual-Luminophore-Doped Silica Nanoparticles for Multiplexed Signaling. *Nano Lett.* **2005**, *5*, 37–43.
38. Ow, H.; Larson, D. R.; Srivastava, M.; Baird, B. A.; Webb, W. W.; Wiesner, U. Bright and Stable Core-Shell Fluorescent Silica Nanoparticles. *Nano Lett.* **2005**, *5*, 113–117.
39. Van Blaaderen, A.; Vrij, A. Synthesis and Characterization of Colloidal Dispersions of Fluorescent, Monodisperse Silica Spheres. *Langmuir* **1992**, *8*, 2921–2931.

40. Wu, C.; Hong, J.; Guo, X.; Huang, C.; Cai, J.; Zheng, J.; Chen, J.; Mu, X.; Zhao, Y. Fluorescent Core-Shell Silica Nanoparticles as Tunable Precursors: Towards Encoding and Multifunctional Nano-Probes. *Chem. Commun.* **2008**, 750–752.
41. Kim, S. H.; Jeyakumar, M.; Katzenellenbogen, J. A. Dual-Mode Fluorophore-Doped Nickel Nitrilotriacetic Acid-Modified Silica Nanoparticles Combine Histidine-Tagged Protein Purification with Site-Specific Fluorophore Labeling. *J. Am. Chem. Soc.* **2007**, *129*, 13254–13264.
42. He, R.; You, X.; Shao, J.; Gao, F.; Pan, B.; Cui, D. Core/Shell Fluorescent Magnetic Silica-Coated Composite Nanoparticles for Bioconjugation. *Nanotechnology* **2007**, *18*, 315601.
43. Bridot, J.-L.; Faure, A.-C.; Laurent, S.; Rivière, C.; Billotey, C.; Hiba, B.; Janier, M.; Josserand, V.; Coll, J.-L.; Vander Elst, L.; et al. Hybrid Gadolinium Oxide Nanoparticles: Multimodal Contrast Agents for in Vivo Imaging. *J. Am. Chem. Soc.* **2007**, *129*, 5076–5084.
44. Hermanson, G. T. *Bioconjugate Techniques*, 2nd edition; Academic Press: London, 2008.
45. Brennan, J. L.; Hatzakis, N. S.; Tshiskudo, T. R.; Dirvianskyte, N.; Razumas, V.; Patkar, S.; Vind, J.; Svendsen, A; Nolte, R. J. M.; Rowan, A. E.; et al. Bionanoconjugation via Click Chemistry: The Creation of Functional Hybrids of Lipases and Gold Nanoparticles. *Bioconjugate Chem.* **2006**, *17*, 1373–1375.
46. Kolb, H. C.; Finn, M. G.; Sharpless, K. B. Click Chemistry: Diverse Chemical Function from a few Good Reactions. *Angew. Chem., Int. Ed.* **2001**, *40*, 2004–2021.
47. Tannous, B. A.; Grimm, J.; Perry, K. F.; Chen, J. W.; Weissleder, R.; Breakefield, X. O. Metabolic Biotinylation of Cell Surface Receptors for In Vivo Imaging. *Nature Methods* **2006**, *3*, 391–396.
48. Diamandis, E. P.; Christopoulos, T. K. The Biotin-(Strept)Avidin System: Principles and Applications in Biotechnology. *Clin. Chem.* **1991**, *37*, 625–63.
49. Patel, S.; Chaffotte, A.; Goubard, F.; Pauthe, E. Urea-Induced Sequential Unfolding of Fibronectin: A Fluorescence Spectroscopy and Circular Dichroism Study. *Biochemistry* **2004**, *43*, 1724–1735.
50. Pauthe, E.; Pelta, J.; Patel, S.; Lairez, D.; Goubard, F. Temperature Induced Beta-Aggregation of Fibronectin. *Biochim. Biophys. Acta* **2002**, *1597*, 12–21.
51. Pelta, J.; Berry, H.; Fadda, G. C.; Pauthe, E.; Lairez, D. Statistical Conformation of Human Plasma Fibronectin. *Biochemistry* **2000**, *39*, 5146–5154.
52. Hoffmann, C.; Leroy-Dudal, J.; Patel, S.; Gallet, O.; Pauthe, E. Fluorescein Isothiocyanate-Labeled Human Plasma Fibronectin in Extracellular Matrix Remodeling. *Anal. Biochem.* **2008**, *372*, 62–71.
53. Le Duc, G.; Roux, S.; Tillement, O.; Perriat, P.; Billotey, C.; Mandon, C.; Mutelet, B.; Alric, C.; Janier, M.; Louis, C. Radio-Sensibilisants à base de Nanoparticules Hybrides d'Oxyde de Lanthanide et Méthode pour Augmenter l'Efficacité Thérapeutique des Radiations par Utilisation de Nanoparticules d'Oxyde de Lanthanides. French Patent, Oct. 16, 2008.
54. Marquette, C. A.; Degiuli, A.; Imbert-Laurenceau, E.; Mallet, F.; Chaix, C.; Mandrand, B.; Blum, L. J. Latex Bead Immobilisation in PDMS Matrix for the Detection of p53 Gene Point Mutation and Anti-HIV-1 Capsid Protein Antibodies. *Anal. Bioanal. Chem.* **2005**, *381*, 1019–1024.
55. Poulouin, L.; Gallet, O.; Rouahi, M.; Imhoff, J.-M. Plasma Fibronectin: Three Steps to Purification and Stability. *Protein Expression Purif.* **1999**, *17*, 146–152.
56. De, G.; Karmakar, B.; Ganguli, D. Hydrolysis-Condensation Reactions of TEOS in the Presence of Acetic Acid Leading to the Generation of Glass-Like Silica Microspheres in Solution at Room Temperature. *J. Mater. Chem.* **2000**, *10*, 2289–2293.